Quaternary International 532 (2019) 23–33

Contents lists available at ScienceDirect

Quaternary International

journal homepage: www.elsevier.com/locate/quaint

The hydrogen isotopic compositions of sedimentary mid-chain n-alkanes record ecological change at a Portuguese paleowetland

Audrey K. Taylor[a,*], Michael M. Benedetti[a], Jonathan A. Haws[b], Chad S. Lane[a]

[a] Department of Earth and Ocean Sciences, University of North Carolina Wilmington, Wilmington, NC, USA
[b] Department of Anthropology, University of Louisville, Louisville, KY, USA

ARTICLE INFO

Keywords:
n-alkane
Wetland
Hydrogen
Isotope
Portugal
Sphagnum

ABSTRACT

The origin of mid-chain (C_{23} and C_{25}) and C_{27} *n*-alkanes in sedimentary archives can be ambiguous. In coastal Portugal, a peat deposit representing a mid-Holocene paleowetland (PRC-South) that was initially dominated by *Sphagnum* presents an ideal setting for assessing methods of mid-chain *n*-alkane source elucidation. In particular, we examine a comprehensive record of the difference in δD between mid-chain (δD_{mid}) and C_{29} *n*-alkanes ($\Delta D_{mid\text{-}C29}$) in relation to *n*-alkane molecular distributions and compound-specific $\delta^{13}C$ values in order to improve interpretations of paleoenvironmental change and evaluate the reliability of δD_{mid} values for hydrologic reconstructions. Mid-chain *n*-alkane production remains significant at PRC-South after a substantial *Sphagnum* decline, yet an increase in $\Delta D_{mid\text{-}C29}$ values indicates a primarily terrestrial origin of mid-chain *n*-alkanes in the upper 50 cm of the deposit. This progression towards more positive $\Delta D_{mid\text{-}C29}$ values coincides with a relative increase in *n*-C_{27} abundance and potentially represents the replacement of *Sphagnum* moss by tree species that produce abundant mid-chain *n*-alkanes, such as *Betula*, *Quercus*, or *Fagus* spp. According to our analysis, $\Delta D_{mid\text{-}C29}$ displays promise as a tool for mid-chain *n*-alkane source attribution in *Sphagnum* paleoenvironments, but interspecies variability of hydrogen isotope fractionation in *Sphagnum* mosses and terrestrial vegetation could critically hinder its application. Our use of $\Delta D_{mid\text{-}C29}$ at PRC-South ultimately exemplifies the importance of accounting for vegetation composition when qualitatively or quantitatively interpreting sedimentary $\delta D_{n\text{-alkane}}$ values, particularly in *Sphagnum* wetlands.

1. Introduction

The hydrogen ($\delta D_{n\text{-alkane}}$) and carbon ($\delta^{13}C_{n\text{-alkane}}$) isotopic compositions of leaf waxes preserved in sedimentary archives, such as *n*-alkanes, have contributed to advancements in our understanding of hydroclimate and vegetation change over time (Sachse et al., 2012; Diefendorf and Freimuth, 2017). The characteristic production of various *n*-alkanes by algae (< *n*-C_{19}), aquatic macrophytes (*n*-C_{21}, *n*-C_{23}, *n*-C_{25}), and terrestrial vegetation (> *n*-C_{25}) can be used to broadly determine organic matter origin (Eglinton and Hamilton, 1967; Ficken et al., 2000), thus relative to bulk organic matter, isotope analyses of these molecules allow for more source-specific interpretations of their isotopic signatures and refined environmental reconstructions (e.g. Feakins, 2013; Lane et al., 2018). While molecular distributions can indicate source, the $\delta^{13}C$ values of leaf waxes can be used to further establish the origin of various homologues in aquatic environments; *n*-alkane production often overlaps across vegetation types and differences in carbon source between submerged macrophytes and terrestrial C_3 plants, for example, produce diagnostic carbon isotope signals (Aichner et al., 2010a; Liu et al., 2015) that can help to resolve some of the ambiguity of *n*-alkane distributions. Reliable source-attribution is especially useful for paleohydrologic investigations, as biosynthetic and evapotranspirative modifications of precipitation δD can vary significantly between vegetation classes (Hou et al., 2007; McInerney et al., 2011; Sachse et al., 2012; Kahmen et al., 2013a, 2013b) and an ambiguous or highly mixed origin of *n*-alkanes can limit their proxy potential (Hepp et al., 2019). Although the apparent offset between meteoric and *n*-alkane δD, typically expressed as $\epsilon_{l/w}$, is species dependent (e.g. Chikaraishi and Naraoka, 2003; Sachse et al., 2006; Hou et al., 2007) and may range between −40 and −200‰ (Sachse et al., 2012), terrestrially-derived sedimentary *n*-alkanes are commonly more D-depleted than precipitation by ~125‰ (Sachse et al., 2004; Liu and An, 2019) and are frequently utilized as a proxy for paleohydrologic processes.

Contrasting $\epsilon_{l/w}$ values between *n*-alkane chain lengths have proven potentially advantageous for evapotranspiration, lake water balance, and relative humidity reconstructions. Modern analyses of lake

* Corresponding author. Present address: Department of Civil and Environmental Engineering and Earth Sciences, University of Notre Dame, IN, USA.
E-mail address: ataylo18@nd.edu (A.K. Taylor).

https://doi.org/10.1016/j.quaint.2019.09.009
Received 1 May 2019; Received in revised form 23 August 2019; Accepted 11 September 2019
Available online 17 September 2019
1040-6182/

ecosystems have demonstrated differing $\epsilon_{l/w}$ values between algal and terrestrially-derived *n*-alkanes, which are primarily attributed to differences in evapotranspirative D-enrichment (Sachse et al., 2004, 2006). Because algal $\epsilon_{l/w}$ is relatively constant across a variety of climates (Sachse et al., 2004, 2006), the δD of algal *n*-alkanes is likely minimally affected by environmental sources of hydrogen fractionation, and the difference in δD between short-chain (algal) and long-chain (terrestrial) *n*-alkanes (ΔD) may be used as a proxy for evapotranspiration (Sachse et al., 2004, 2006). Based on this concept, the ΔD between aquatic, mid-chain and terrestrial, long-chain *n*-alkanes, or a dual-biomarker approach (Rach et al., 2017), has been applied to lake sediments to estimate changes in paleohydrology (Mügler et al., 2008; Rach et al., 2014, 2017). Mügler et al. (2008) proposed that the direction of difference in δD (+/−) between terrestrial and aquatic *n*-alkanes could be indicative of catchment hydrology, given that submerged macrophytes record the δD of their water catchment and generally produce *n*-alkanes depleted in D relative to terrestrial vegetation, unless evaporation of lake water exceeds precipitation. In humid environments, the minimal evaporation of lake water may permit the use of the dual biomarker approach to similarly estimate relative humidity (Rach et al., 2017). However, results from paleoenvironmental applications of this lake water balance reconstruction technique and dual biomarker approach are potentially complicated by vegetation isotope effects, inexplicit *n*-alkane origin, and insufficient multi-homologue *n*-alkane abundances (Aichner et al., 2010b; Rao et al., 2014; Rach et al., 2017; Hepp et al., 2019).

Analyses and applications of the ΔD proxy have primarily focused on lake ecosystems (e.g. Sachse et al., 2004, 2006; Mügler et al., 2008; Aichner et al., 2010b; Rao et al., 2014). The utilization of ΔD in bogs and peatlands could provide valuable records of paleohydrology, but sedimentary mid-chain *n*-alkanes (n-C_{23} and n-C_{25}) in these depositional settings are often representative of *Sphagnum* mosses rather than aquatic vegetation. *Sphagnum* mosses are non-vascular species that, unlike algae or aquatic plants, are especially susceptible to evaporative modifications of meteoric δD (Nichols et al., 2010), likely hindering the use of ΔD between middle and long-chain *n*-alkanes to directly quantify terrestrial evapotranspiration or wetland hydrology in *Sphagnum* paleoenvironments. Alternatively, ΔD may provide valuable insight into the sources of mid-chain *n*-alkanes in wetland ecosystems, as demonstrated offsets between *Sphagnum* and terrestrial vegetation $\epsilon_{l/w}$ are largely attributed to microclimate and biosynthetic differences (Sachse et al., 2006; Nichols et al., 2010) and some analyses have demonstrated ample production of mid-chain *n*-alkanes by terrestrial vegetation (Sachse et al., 2006; Balascio et al., 2018). As a result, δD_{mid} in *Sphagnum* bogs and peatlands is likely hypersensitive to vegetation change and potentially unreliable for paleonvironmental reconstructions, even if n-C_{23} or n-C_{25} is the most abundant homologue. The use of ΔD to determine mid-chain *n*-alkane origin and its variability could improve interpretations of molecular distributions and $\delta^{13}C_{n\text{-alkane}}$ values and further be used as a tool for assessing the reliability of *Sphagnum*-derived *n*-alkanes as climatic indicators in specific locales.

During the mid-Holocene, *Sphagnum* moss briefly occupied a wetland at Praia Rei Cortiço (PRC) along the Portuguese coast, but did not persist likely due to precipitation variability in this ecotonal region (Taylor et al., 2018). The initial predominance and subsequent rapid decline of *Sphagnum* at PRC presents the opportunity to apply and assess ΔD as a tool for mid-chain *n*-alkane source elucidation. While Taylor et al. (2018) focused on paleoclimate interpretation, here we examine the utility of ΔD and its implications for the paleoenvironment of PRC. We analyze a comprehensive record of the difference in δD between mid-chain and C_{29} *n*-alkanes ($\Delta D_{mid\text{-}C29}$) in relation to *n*-alkane abundances and compound-specific $\delta^{13}C_{n\text{-alkane}}$ values in order to differentiate between *Sphagnum* and terrestrial *n*-alkane contributions to the organic matter pool at PRC and additionally evaluate the reliability of different *n*-alkane chain lengths for hydrologic reconstructions of *Sphagnum* wetlands.

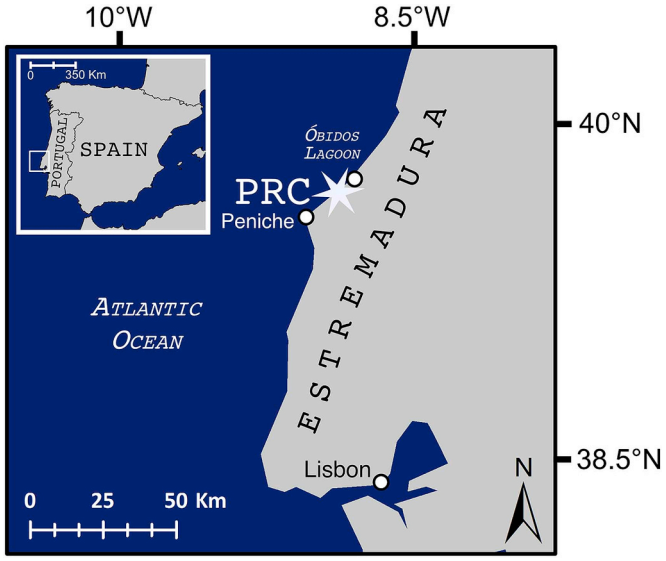

Fig. 1. Location of our study area, Praia Rei Cortiço (PRC), along the Estremadura coast in Portugal.

2. Regional setting

Praia Rei Cortiço (PRC) is positioned along the central Portuguese coast at approximately 39°N near the mouth of the Óbidos lagoon (Fig. 1). Climate in this region of Portugal is classified as sub-humid Mediterranean (Cfb), with maximum rainfall in winter. Modern vegetation at the site consists of *Juniperus* spp., *Quercus* spp., and various shrubs and herbs such as Ericaceae and Cyperaceae (Minckley et al., 2015). PRC is situated at an intermediate and dynamic location between temperate Atlantic forest and Mediterranean steppe and is likely hypersensitive to environmental change (Taylor et al., 2018).

Coastal deposits at PRC have contributed to an improved paleoenvironmental (Minckley et al., 2015; Taylor et al., 2018), archaeological (Haws et al., 2010), and geomorphological (Benedetti et al., 2009) history of this region. Of particular interest is the pollen analysis of a riparian organic deposit dating to approximately 100–80 ka that was used to reconstruct climate and vegetation during Marine Isotope Stages 5a–5d, part of the last interglacial complex (Minckley et al., 2015). Minckley et al. (2015) determined that PRC was previously dominated by Ericaceae and *Pinus* spp. with smaller communities of *Quercus* spp. and wetland taxa such as Cyperaceae and Poaceae.

A similar organic fill, referred to here as PRC-South (Fig. 2), represents a comparable mid-Holocene (6.6–5.4 ka) riparian wetland that is preserved 300 m south of the interglacial deposit. The 2 m thick deposit outcrops at 4–6 m above mean sea level between an underlying fluvial channel deposit and overlying aeolian sand (Fig. 2; Taylor et al., 2018). At PRC-South, compound-specific isotope compositions and molecular distributions of *n*-alkanes were utilized to document regional hydroclimate variability and rapid vegetation change during the wetland's brief mid-Holocene existence at PRC (Taylor et al., 2018). Given evidence of abundant *Sphagnum* moss, the coastal setting, and the paleoenvironmental history of PRC, Taylor et al. (2018) hypothesize that the PRC-South wetland was likely similar in morphology and vegetation composition to that of the Rivatehilos of Doñana National Park in southwestern Spain. The Rivatehilos peat bogs are composed of vegetation that is more characteristic of the northwestern Iberian margin, such as *S. inundatum* and *Erica ciliaris* wet heathland, and have been drastically reduced in size over the past century due to anthropogenic pressures (Sousa et al., 2012).

Fig. 2. The Praia Rei Cortiço mid-Holocene organic fill (PRC-South) in relation to the coast and underlying Cretaceous bedrock (left) and an enlarged image of the sampled section of PRC-South (right).

3. Materials & methods

3.1. PRC-south

Stratigraphic and chronological methods and results for the 2 m thick PRC-South organic fill are presented in detail in Taylor et al. (2018). Briefly, PRC-South is mostly comprised of organic matter (0.85–70.3%) and sand content (11.5–98.5%) that varies throughout the deposit and defines the stratigraphic zonation of PRC-South (Taylor et al., 2018). Chronology of the deposit was established by two radiocarbon dates and further constrained by two optically stimulated luminescence (OSL) ages. A charcoal sample at 40 cm and a wood sample at 171 cm submitted to Beta Analytic, Inc provided ^{14}C dates of 5605 ± 25 cal BP and 6405 ± 40 cal BP (Fig. 2), respectively (Taylor et al., 2018). The OSL samples from 30 cm and below the deposit at 215 cm were analyzed at the Luminescence Dating Research Laboratory, University of Illinois-Chicago and returned dates of 5170 ± 470 ka and 7490 ± 655 ka (Fig. 2), respectively, providing additional age model confirmation (Taylor et al., 2018). Given these results, the PRC-South organic fill is estimated to represent the time period between 5.38 ka and 6.58 ka (Taylor et al., 2018).

3.2. Compound extraction

The PRC-South deposit was sampled at 10–cm intervals for compound-specific isotope and *n*-alkane molecular analyses and at 2–cm intervals for bulk sedimentary isotopic analyses. Compounds were extracted from a total of 21 sediment samples. Dried and ground sediment samples were initially sealed in Teflon™ bottles in a 2:1 mixture of DCM and MeOH and placed on a shaker table overnight. The total lipid extract was base saponified and the remaining lipids were separated into neutral and polar fractions using silica-gel columns with DCM and MeOH as eluting solvents, respectively. Urea adduction was subsequently used to further purify the resultant aliphatic extract.

3.3. Compound identification and quantification

Alkanes were identified and quantified in our urea adducted fraction using a Thermo 1310 gas chromatograph coupled with an ISQ quadrupole mass spectrometer and flame ionization detector. Compounds were separated on a Thermo TG-5 SILMS silica column (30 m, 0.32 mm i.d., 0.32 μm thickness) with the GC oven temperature programmed for 70 °C isothermal for 1 min, 20 °C/min to 180 °C, 4 °C/min to 320 °C, 320 °C isothermal for 5 min, 30 °C/min to 350 °C, and 350 °C isothermal for 1 min. An external standard including *n*-C_4–*n*-C_{40} from Supelco was used to assign and quantify *n*-alkanes.

P_{aq} is used to generally approximate organic matter inputs from submerged aquatic macrophytes (Ficken et al., 2000), but can also reflect relative *Sphagnum* moss abundance due to its similarly abundant production of *n*-C_{23} and *n*-C_{25} (Nichols et al., 2006). To better represent the *Sphagnum* moss species apparent at PRC-South, we examine a modification of the Ficken et al. (2000) equation that includes the C_{27} *n*-alkane:

$$P_{aq27} = (C_{23} + C_{25} + C_{27})/(C_{23} + C_{25} + C_{27} + C_{29} + C_{31})$$

We also calculate $ACL_{29\text{-}33}$ to exclude *Sphagnum* influence and isolate terrestrial vegetation changes:

$$ACL_{29-33} = (29{*}C_{29} + 31{*}C_{31} + 33{*}C_{33})/(C_{29} + C_{31} + C_{33})$$

The Carbon Preference Index (CPI) can be used to determine the primary source of sedimentary *n*-alkanes more broadly, with values > 1 indicating a predominance of odd over even *n*-alkanes and a terrestrial plant origin, and values < 1 indicating the reverse and a diagenetic or microbial origin. CPI, also sometimes referred to as odd over even predominance (OEP), has been used as a degradation proxy (e.g. Zech et al., 2013), but can also be influenced by changes in vegetation due to differences in *n*-alkane production among higher plants (Bush and McInerney, 2013). We calculated CPI as follows (Marzi et al., 1993):

$$CPI = \left[\sum_{odd}(C_{21} - C_{31}) + \sum_{odd}(C_{23} - C_{33})\right] / \left[2\sum_{even}(C_{22} - C_{32})\right].$$

3.4. Compound-specific isotope analyses

The carbon and hydrogen isotopic compositions of *n*-alkanes were determined at the University of North Carolina Wilmington using a Thermo Delta V Plus mass spectrometer interfaced with a Thermo Trace 1310 gas chromatograph via an Isolink II device. Samples were injected with a Thermo AI1310 autosampler at 320 °C in surged splitless mode and separated on a RTX-5 silica column (60 m, 0.25 mm i.d., 0.50 μm thickness) using the following GC temperature programming: 70 °C isothermal for 1 min, 20 °C/min to 180 °C, 5 °C/min to 320 °C, and 320 °C isothermal for 20 min. Samples were analyzed in duplicate to determine measurement precision, and the Indiana University B4 *n*-alkane mixture was injected after every four samples to monitor instrument precision. The standard deviations of B4 over the course of this study were < 0.35‰ and < 5‰ for carbon and hydrogen, respectively. The uncertainty calculator spreadsheet produced by Polissar and D'Andrea (2014) was used to correct raw data to the VSMOW and VPDB scales and calculate propagated errors of isotopic values.

For ΔD analyses, *n*-C_{23}, *n*-C_{25}, and *n*-C_{27} are considered individually and '$\Delta D_{mid\text{-}C29}$' refers to these calculations collectively, whereas '$\Delta D_{avg\text{-}}$

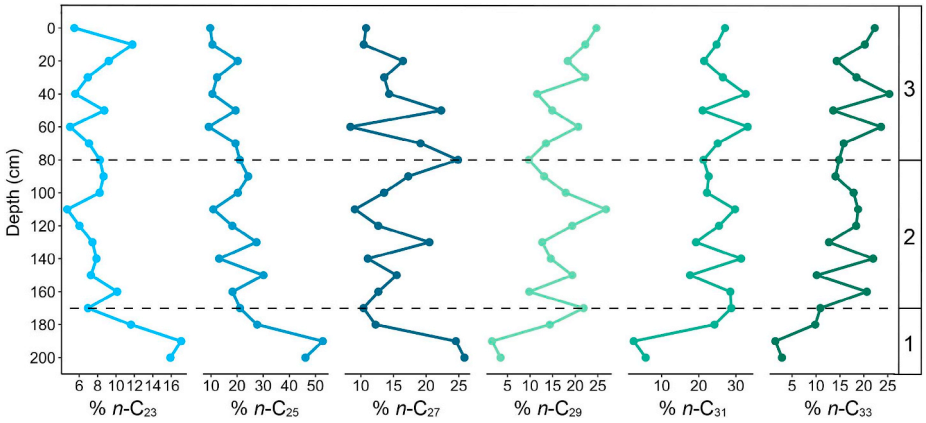

Fig. 3. Relative abundance (%) of odd *n*-alkanes (*n*-C_{23}–*n*-C_{33}) in each stratigraphic zone of PRC-South. Note the variable x-axis scale.

$_{C29}$' displays aggregated mid-chain (including *n*-C_{27}) δD values:

$$\Delta D_{C23-C29} = \delta D_{n-C23} - \delta D_{n-C29}$$

$$\Delta D_{C25-C29} = \delta D_{n-C25} - \delta D_{n-C29}$$

$$\Delta D_{C27-C29} = \delta D_{n-C27} - \delta D_{n-C29}$$

$$\Delta D_{avg-C29} = [(\delta D_{n-C23} * \delta D_{n-C25} * \delta D_{n-C27})/3] - \delta D_{n-C29}$$

4. Results

4.1. n-Alkane distributions

The distribution of odd-numbered *n*-alkanes is highly variable throughout the stratigraphy of the PRC-South deposit. Distinct trend divergence between mid-chain (C_{23}, C_{25}, and C_{27}) and long-chain (C_{29}, C_{31}, C_{33}) *n*-alkanes is apparent across all zones, designated according to stratigraphy by Taylor et al. (2018), with relative mid-chain and *n*-C_{27} abundances generally decreasing and longer-chain *n*-alkane abundances generally increasing over time (Fig. 3). In Zone 1 (200–170 cm), molecular distributions of *n*-alkanes are initially dominated by *n*-C_{25} (> 46%) followed by *n*-C_{27} (> 24%) and *n*-C_{23} (> 15%), and *n*-C_{29}, *n*-C_{31}, and *n*-C_{33} compose a comparatively minor fraction of the sedimentary *n*-alkanes (< 15% combined; Figs. 3 and 4). Combined mid-chain and *n*-C_{27} abundance decreases from ~183 to ~18 μg/g TOC in Zone 1, whereas long-chain *n*-alkanes do not display a distinct trend and fluctuate between ~7 and 38 μg/g TOC (Fig. S1). In Zone 2 (170–80 cm), mid-chain and C_{27} *n*-alkane relative abundances decrease significantly and *n*-C_{25} and *n*-C_{31} alternate as the predominant alkane, with an exception at 80 cm where *n*-C_{27} is most abundant (Fig. 4). The combined relative abundance of mid-chain and C_{27} *n*-alkanes in Zone 2 fluctuates between 32% and 55%, whereas the combined relative abundance of terrestrial long-chain *n*-alkanes fluctuates between 44% and 75% (Figs. 3 and 4). The concentration of long-chain *n*-alkanes is generally greater in Zone 2 than in Zone 1, ranging between 7.9 and 56 μg/g TOC, and the combined concentration of mid-chain and C_{27} *n*-alkanes fluctuates between 2.6 and 52 μg/g TOC (Fig. S1). In Zone 3 (80–0 cm), *n*-C_{27} and *n*-C_{31} alternate as the predominant alkane and the distribution of mid-chain *n*-alkanes becomes more variable (Fig. 4). Long-chain *n*-alkanes become generally more abundant in Zone 3, with a combined relative abundance ranging between 45% and 77% and absolute abundances ranging between 1.9 and 151 μg/g TOC (Figs. 3 and 4, and Fig. S1). Mid-chain, C_{27}, and long-chain *n*-alkane concentrations display similar trends in Zone 3 (Fig. S1).

Although *n*-C_{27} is not typically considered a mid-chain *n*-alkane, we classify it as such throughout the rest of the manuscript because of its relation to the *Sphagnum*-dominated zone and overall correspondence to molecular trends of *n*-C_{23} and *n*-C_{25} (Fig. 3). As such, we present P_{aq27}, a modified form of P_{aq} which considers *n*-C_{27}, to more accurately document *Sphagnum* presence and abundance at PRC-South. P_{aq27} is nearly identical to P_{aq} presented by Taylor et al. (2018), but displays a larger range (0.05–0.96; Fig. 5). Maximum P_{aq27} values occur in Zone 1 and, although variable throughout the deposit, generally decrease towards the top of the deposit, reaching minimum values in Zone 3.

The $ACL_{29\text{-}33}$ values are also variable throughout the PRC-South deposit, fluctuating between 30.6 and 31.4 (Fig. 5). In Zone 1, $ACL_{29\text{-}33}$

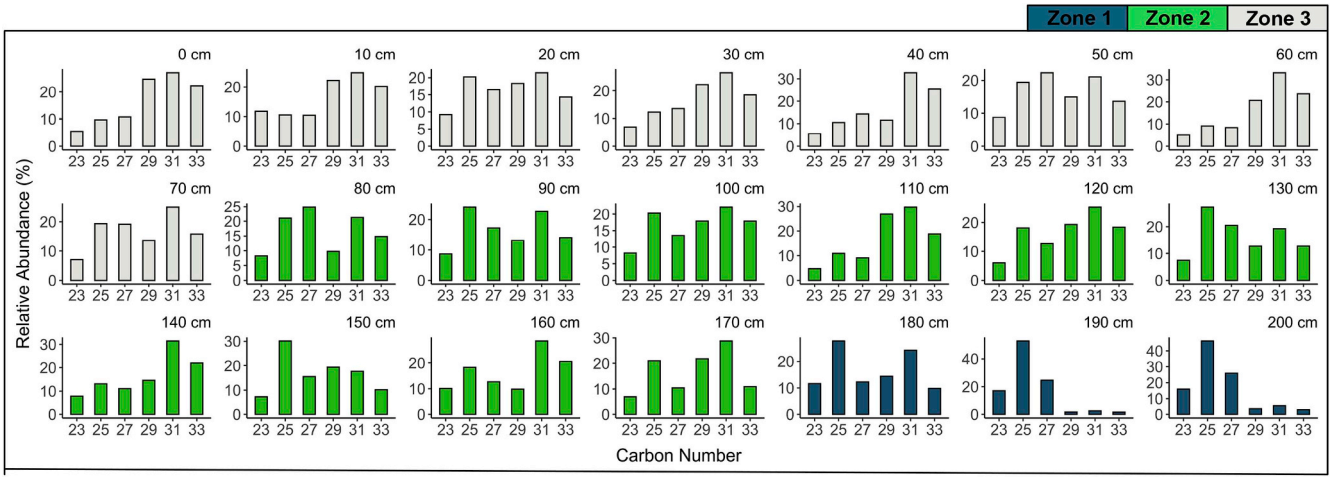

Fig. 4. The molecular distribution of odd *n*-alkanes (*n*-C_{23}–*n*-C_{33}) in each stratigraphic zone of PRC-South. Note the variable y-axis scale.

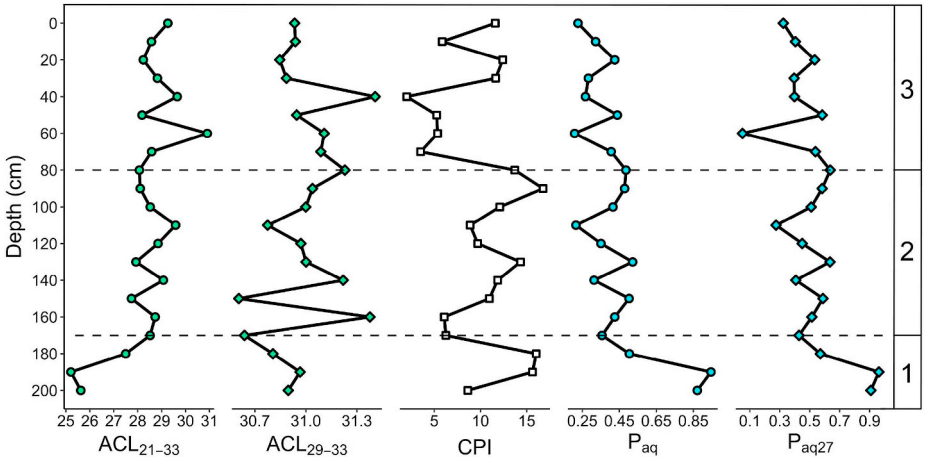

Fig. 5. Molecular proxies of *n*-alkane origin at PRC-South including $ACL_{21\text{-}33}$, CPI, and P_{aq} presented in Taylor et al. (2018), and modified proxies, $ACL_{29\text{-}33}$ and P_{aq27}, which are primarily used to assess controls on $\Delta D_{mid\text{-}C29}$.

resembles P_{aq27} (Fig. 5), with values generally decreasing, but represents a relatively minimal overall change of 0.3. $ACL_{29\text{-}33}$ values are the most variable in Zone 2 (80–170 cm), ranging from 30.6 to 31.2, and demonstrate notable fluctuations between 140 and 170 cm (Fig. 5). In Zone 3, $ACL_{29\text{-}33}$ values display an overall decrease towards the top of the deposit, but return to a relatively high value of 31.4 at 50 cm (Fig. 5; Table S1).

The CPI values fluctuate between 2.02 and 16.77, with relatively high CPI values occurring throughout Zones 1 and 2 and generally lower CPI values in Zone 3 (Fig. 5). CPI displays some trend similarities to $ACL_{29\text{-}33}$ in Zone 3 and to the other molecular *n*-alkane proxies ($ACL_{21\text{-}33}$, P_{aq}, P_{aq27}) in Zones 1 and 2 (Fig. 5).

4.2. Compound-specific $\delta^{13}C$ values

Sedimentary $\delta^{13}C_{n\text{-alkane}}$ values are generally similar across homologues, but display some differences in trend between mid- and long-chain *n*-alkanes (Fig. 6). The $\delta^{13}C$ values of each *n*-alkane have ranges of approximately 2‰–4.5‰, with *n*-C_{27} displaying the largest range and *n*-C_{23} the smallest. In Zone 1, the $\delta^{13}C$ values of mid-chain *n*-alkanes fluctuate minimally between −31.2‰ and −32.6‰, although values for *n*-C_{25} and *n*-C_{27} at 190 cm are unavailable. Long-chain *n*-alkanes are notably more depleted in ^{13}C than mid-chain *n*-alkanes, and display an overall increase throughout Zone 1, ranging from −33.4‰ to −31‰ and −34.5‰ to −31.2‰ for *n*-C_{29} and *n*-C_{31}, respectively. In Zone 2, $\delta^{13}C_{n\text{-alkane}}$ values are fairly consistent across all homologues, with values ranging between −30.1 and −32.4 throughout the zone. Zone 3 $\delta^{13}C_{n\text{-alkane}}$ values are relatively variable and decrease overall. Absolute $\delta^{13}C_{n\text{-alkane}}$ values remain similar between middle and long chain-lengths in Zone 3, ranging from −32.7‰ to −27.6‰ and −32.9‰–29.8‰, respectively, but have distinct trend dissimilarities around 60 cm and opposing signals in the upper section of the deposit (Fig. 6). Mid-chain *n*-alkanes show a relatively large increase in $\delta^{13}C$ values between 80 and 60 cm that is reflected to a smaller extent only by *n*-C_{29} and not by *n*-C_{31} (Fig. 6).

4.3. Compound-specific δD values

The δD values of all *n*-alkanes at PRC-South (*n*-C_{23}–*n*-C_{31}) follow fairly similar trends, though there are distinct points of divergence between middle and long-chain *n*-alkanes (Fig. 7). The δD values of *n*-C_{29} and *n*-C_{31} range 53.5‰ and 49.2‰, respectively, whereas *n*-C_{23}, *n*-C_{25}, and *n*-C_{27} δD values are more variable with ranges of 140.3‰, 89.4‰, and 66‰, respectively. On average, *n*-C_{23}, *n*-C_{25}, and *n*-C_{27} are 33‰, 46‰, and 32‰ more depleted in D than *n*-C_{29}. Noteworthy contrasts and substantial differences in δD between middle and long chain-lengths occur in Zone 1 and at 60 cm (Fig. 7). The *n*-C_{23} homologue displays significant divergence from the general trend at 30 cm, but the analytical precision is good with a standard deviation of less than 2.5‰ between measurements.

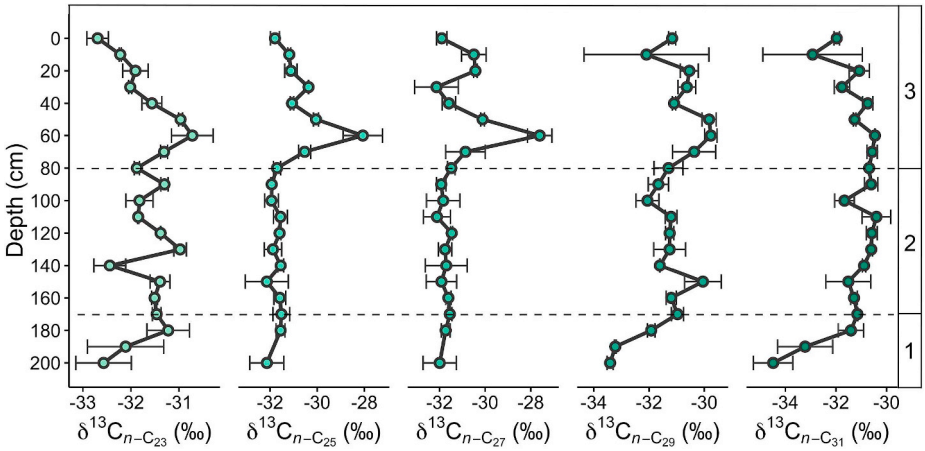

Fig. 6. Compound-specific $\delta^{13}C$ values of odd *n*-alkanes between *n*-C_{23} and *n*-C_{31} extracted from PRC-South. Error bars represent one standard deviation of replicate analyses.

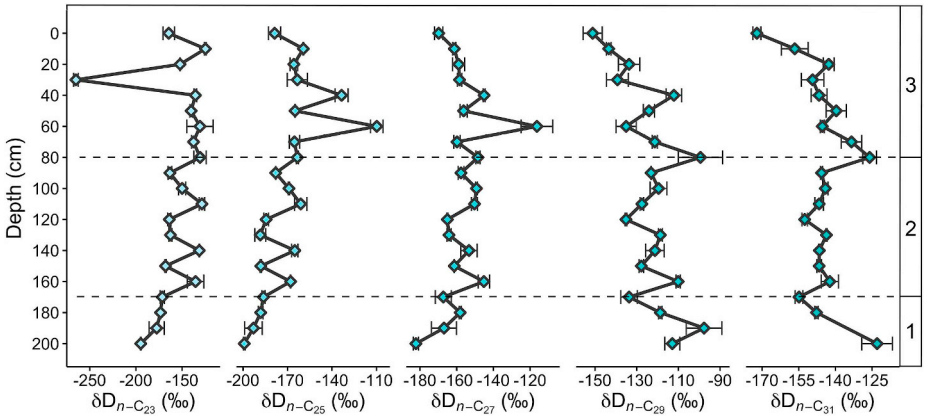

Fig. 7. Compound-specific δD values for odd *n*-alkanes between *n*-C_{23} and *n*-C_{31} extracted from PRC-South. Error bars represent one standard deviation of replicate analyses. Note the variable x-axis scale.

4.4. $\Delta D_{mid\text{-}C29}$

Values of $\Delta D_{mid\text{-}C29}$ vary significantly throughout the PRC-South deposit, but overall individual homologues reflect very similar trends (Fig. 8). The $\Delta D_{C23\text{-}C29}$ values have the largest range, varying between −125.7‰ and 18.8‰, and $\Delta D_{C25\text{-}C29}$ and $\Delta D_{C27\text{-}C29}$ values range from −95.3‰ to 25.3‰ and −69.3‰–18.9‰, respectively (Fig. 8; Table S1). Each $\Delta D_{mid\text{-}C29}$ series displays a strong and significant correlation to molecular proxies of vegetation change which consider mid-chain *n*-alkane abundances (P_{aq}, P_{aq27}), but does not correspond to $ACL_{29\text{-}33}$ (Fig. 9). Notably, the relation between $\Delta D_{C25\text{-}C29,\ C27\text{-}29}$ and P_{aq27} is stronger than the relation to P_{aq} (Fig. 9).

5. Discussion

5.1. Paleoenvironmental change at PRC-South

Molecular and isotopic evidence presented by Taylor et al. (2018) indicate substantial changes in vegetation composition at PRC-South primarily driven by the climate-induced reduction of *Sphagnum* moss during the mid-Holocene. A combination of high relative *n*-C_{23}, *n*-C_{25}, and *n*-C_{27} abundances and related high P_{aq} values (> 0.8), $\delta^{13}C$ values of mid-chain and C_{27} *n*-alkanes that are ~31‰ on average, and sedimentary C/N ratios of approximately 50 document an initial predominance of *Sphagnum* moss between 6.6 and 6.5 ka (Taylor et al., 2018). The Iberian Peninsula represents the southernmost limit of *Sphagnum's* ecological range in Europe, and modern *Sphagnum* wetlands are uncommon in the region. However, many species of *Sphagnum* do inhabit the peninsula and are more common in the high altitudes of mountainous areas and coastal zones (Seneca, 2003). *Sphagnum* species from the Subsecunda and Acutifolia sections are among the most abundant in Portugal, and *S. auriculatum* and *S. subnitens*, in particular, occupy the Estremadura region (Seneca, 2003). The *n*-alkane distribution of *n*-C_{25} > *n*-C_{27} > *n*-C_{23} at PRC-South during *Sphagnum* predominance likely represents a species similar to *S. fimbriatum* (Baas et al., 2000; Bingham et al., 2010; Taylor et al., 2018), which is part of the Acutifolia section common to the region.

Following a reduction in precipitation after 6.5 ka, a substantial decrease in P_{aq} from 0.95 to 0.36 over the course of ~100 years marks a significant *Sphagnum* decline at PRC-South (Taylor et al., 2018). Additionally, a simultaneous ~25 decrease in C/N values likely reflects greater peat aeration and decomposition as a result of *Sphagnum* loss (Taylor et al., 2018). This drastic reduction in *Sphagnum* and continued variability of vegetation composition throughout the mid-Holocene at PRC-South presents an ideal case study to evaluate the influence of shifting mid-chain and C_{27} *n*-alkane origin on sedimentary δD values and the viability of source elucidation of *n*-alkanes using ΔD.

5.2. Evaluation of $\Delta D_{mid\text{-}C29}$

Offsets between the hydrogen isotopic composition of mid-chain and long-chain *n*-alkanes at PRC-South are most likely reflective of differential biosynthetic fractionations in *Sphagnum* mosses and terrestrial plants. Nichols et al. (2010) demonstrated an approximate

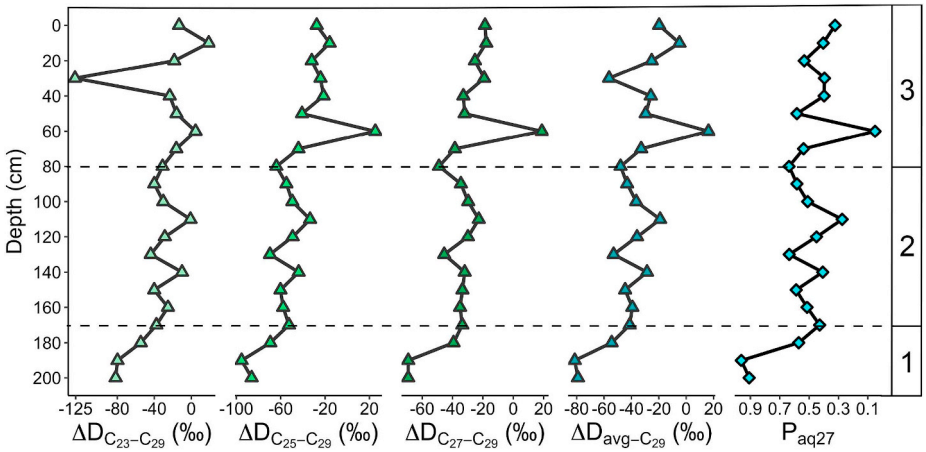

Fig. 8. Each $\Delta D_{mid\text{-}C29}$ series in relation to P_{aq27}, representing *Sphagnum* moss abundance, at PRC-South. ΔD_{avg}-C_{29} illustrates the difference between aggregated mid-chain δD and $\delta D_{n\text{-}C29}$ values.

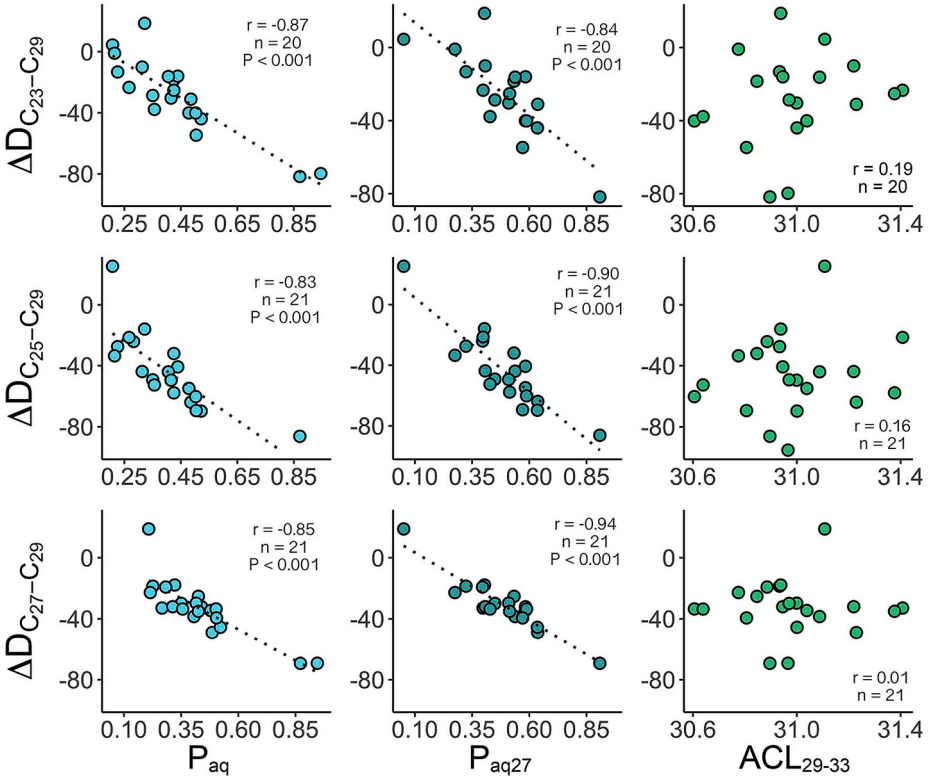

Fig. 9. The statistical relationships between each $\Delta D_{mid\text{-}C29}$ series and molecular proxies of relative *Sphagnum* abundance, P_{aq} (Taylor et al., 2018) and P_{aq27}, and terrestrial vegetation change ($ACL_{29\text{-}33}$). For statistical analyses related to $\Delta D_{C23\text{-}C29}$, the anomalous value at 30 cm is excluded.

biosynthetic fractionation of 175‰ between source water and *n*-C_{23} δD in *Sphagnum* species. Assuming a mean terrestrial $\epsilon_{l/w}$ of 100‰, Nichols et al. (2010) determined that *Sphagnum* mosses produce $\delta D_{n\text{-alkane}}$ values that are roughly 75‰ more negative than terrestrial $\delta D_{n\text{-alkane}}$ values, which is consistent with overall more negative mid-chain $\delta D_{n\text{-alkane}}$ values relative to long-chain $\delta D_{n\text{-alkane}}$ values at PRC-South. This apparent hydrogen isotopic offset between *Sphagnum* and terrestrial plant lipids, in combination with mutual mid-chain *n*-alkane production and a largely terrestrial source of long-chain *n*-alkanes, permits the use of ΔD to isolate the effects of vegetation change and discern mid-chain *n*-alkane origin.

Most *Sphagnum* species produce relatively inconsequential amounts of long-chain *n*-alkanes (Baas et al., 2000; Nott et al., 2000), and it is unlikely that δD values of long-chain *n*-alkanes have been markedly modified by changes in *Sphagnum* abundance. However, there are several *Sphagnum* species that have bimodal *n*-alkane distributions that include or maximize at *n*-C_{31} (Bingham et al., 2010; Balascio et al., 2018) and others that still produce *n*-C_{31} in considerable amounts (Baas et al., 2000; Nott et al., 2000; Nichols et al., 2006). Although molecular and isotopic trends of *n*-C_{31} at PRC-South correspond clearly with *n*-C_{29} and appear to diverge from middle chain-lengths (Fig. 3), we focus on the use of *n*-C_{29} to avoid potential source overlap that could diminish interpretations of ΔD for mid-chain *n*-alkane source elucidation.

At PRC-South, we interpret more negative $\Delta D_{mid\text{-}C29}$ values to represent a greater relative contribution of D-depleted, *Sphagnum*-derived mid-chain *n*-alkanes to the sedimentary organic matter pool. Conversely, more positive $\Delta D_{mid\text{-}C29}$ values are interpreted as an increased contribution of D-enriched, terrestrial-derived mid-chain *n*-alkanes to the sedimentary organic matter pool. Despite the more negative δD values of *Sphagnum*-derived *n*-alkanes, *Sphagnum* mosses utilize water from within their hyaline cells that is subjected to greater evaporative D-enrichment than the acrotelm water that is used by terrestrial vegetation (Nichols et al., 2010), and temporal changes in evaporation may also influence $\Delta D_{mid\text{-}C29}$ values. Differential evaporative enrichment of source water is also considered in interpretations of $\Delta D_{mid\text{-}C29}$, although the isotopic effects of variable *n*-alkane origin are likely more substantial at PRC-South given the magnitude of change observed.

The strong and significant correlation between $\Delta D_{mid\text{-}C29}$ and molecular indices of *Sphagnum* moss at PRC-South (Fig. 9) indicates that it is most probable that the dissimilarities and opposing trends between middle and long-chain $\delta D_{n\text{-alkane}}$ values can be attributed to changes in relative *Sphagnum* abundance at PRC-South that obstruct the climatic isotope signal recorded by δD_{mid} values. The lack of correspondence between $\Delta D_{mid\text{-}C29}$ and the terrestrial vegetation index, $ACL_{29\text{-}33}$, indicates that changes in terrestrial vegetation composition likely have minimal influence on $\Delta D_{mid\text{-}C29}$ values at PRC-South (Fig. 9), and *Sphagnum* decline is the principal cause for variations in $\Delta D_{mid\text{-}C29}$ over time. The notable shift in δD_{mid} values from 190 to 170 cm (Fig. 7) is likely the result of the substantial reduction in *Sphagnum* and consequent relative increase in terrestrially-derived, comparatively D-enriched sedimentary mid-chain *n*-alkanes, evidenced by a decrease in P_{aq27} from 0.96 to 0.43, and is further reflected by a near 40‰ advance towards more positive $\Delta D_{mid\text{-}C29}$ values (Fig. 8). From 70 to 60 cm, opposing δD values between middle and long-chain *n*-alkanes represent a positive $\Delta D_{mid\text{-}C29}$ excursion ranging between ~20‰ and ~68‰, depending on mid-chain *n*-alkane (Fig. 8; Table S1), and similarly correspond to a significant reduction in P_{aq27} from 0.54 to 0.05 (Fig. 8; Table S1). Although the decline in *Sphagnum* is likely due to increased aridity (Taylor et al., 2018) and enhanced evaporation of *Sphagnum* source water may have contributed to the more positive $\Delta D_{mid\text{-}C29}$ values, these changes in *n*-alkane origin were likely more influential on δD_{mid} values given the large isotopic offset (> 65‰) between terrestrial vegetation and *Sphagnum* moss that is evident in Zone 1 (Fig. 8). While not *Sphagnum* dominated, Seki et al. (2009) observed a similar relationship between $\delta D_{n\text{-alkane}}$ dissimilarities and P_{aq} in a northeastern China peat bog and determined that ΔD was reflective of variable mid-chain *n*-alkane origin due to vegetation change.

Conclusions about the isotopic effects of relatively large environmental changes may be drawn from analysis of δD_{mid} values and *n*-alkane molecular proxies alone, however it is important to note the subtler changes that do not appear to affect δD_{mid} but are apparent upon examination of $\Delta D_{mid\text{-}C29}$. In the upper 50 cm, $\delta D_{n\text{-alkane}}$ values of all chain-lengths, excluding *n*-C_{23}, generally decrease towards the top of the deposit (Fig. 7). An underlying shift in $\delta D_{n\text{-}C25}$ and $\delta D_{n\text{-}C27}$ values is discerned by a progression towards considerably higher $\Delta D_{mid\text{-}C29}$ values that corresponds to a 0.26 decrease in P_{aq27}. Values of $\Delta D_{C25\text{-}C29}$ range between −40.8‰ and −15.8‰ and $\Delta D_{C27\text{-}C29}$ values range between −32.1‰ and −17.8‰ in this subsection of Zone 1 (Fig. 8; Table S1). Likewise, in Zone 2, $\delta D_{n\text{-alkane}}$ trends are relatively consistent across homologues (Fig. 7) and changes in *n*-alkane molecular proxies are moderate relative to the rest of the deposit, but $\Delta D_{mid\text{-}C29}$ values vary accordingly (Fig. 8). These modifications of δD_{mid} values resulting from the combined effects of variable meteoric water δD and comparatively minimal changes in organic matter contribution, as demonstrated by $\Delta D_{mid\text{-}C29}$ and *n*-alkane abundances, emphasize the sensitivity of mid-chain *n*-alkane δD to locale-specific changes in vegetation composition.

5.3. Paleoenvironmental implications of $\Delta D_{mid\text{-}long}$ at PRC-South

In general, increasing $\Delta D_{mid\text{-}C29}$ values towards the top of the deposit indicate an increasingly terrestrial plant origin of mid-chain *n*-alkanes at PRC-South. The C_{23} *n*-alkane is the most abundant homologue among mid-chain *n*-alkanes at 10 cm, which is an anomalous distribution at PRC-South (Fig. 4). Despite *n*-C_{23} being present at a similar relative abundance (~10%) to depths where *Sphagnum* moss was likely still a prominent component of the landscape, such as 170 cm or 180 cm in Zone 1, it is likely terrestrially-derived (Figs. 3 and 4). The $\Delta D_{C23\text{-}C29}$ value at this depth is 18.8‰, which is a > 50‰ increase relative to lower depths with nearly equivalent relative *n*-alkane abundances (Figs. 3, 5 and 8). This larger shift and the overall more positive $\Delta D_{C23\text{-}C29}$ values compared to the other mid-chain *n*-alkanes could be related to the comparably small production of *n*-C_{23} by the *Sphagnum* moss at PRC-South and a resultant increased sensitivity to terrestrial contributions. At 20 cm we observe a similar shift, *n*-C_{25} is the most abundant mid-chain *n*-alkane, identical to *Sphagnum*-dominated zones, and among all homologues is second only to *n*-C_{31} by a small margin (< 1.5%; Figs. 3 and 4). However, $\Delta D_{C25\text{-}C29}$ is ~30‰ more positive than depths with similar relative *n*-alkane abundances in Zone 1 (Figs. 3, 4 and 8). Without $\Delta D_{mid\text{-}C29}$, these molecular distributions in Zone 3 could be misinterpreted as indicators of *Sphagnum* moss organic matter contributions. Vegetation composition at PRC-South in Zone 3 is markedly different from Zone 1 according to $\Delta D_{mid\text{-}C29}$, however, and *Sphagnum* was likely not the principal source of mid-chain homologues in the upper 50 cm of the deposit.

This progression towards higher $\Delta D_{mid\text{-}C29}$ values in Zone 3 coincides with an increase in *n*-C_{27} abundance relative to other mid-chain *n*-alkanes, and *n*-C_{27} is the most abundant middle chain-length throughout most of the upper 80 cm of the PRC-South deposit (Figs. 3 and 4). Some tree species are significant terrestrial sources of mid-chain *n*-alkanes and multiple genera typical of this region abundantly produce *n*-C_{23}, *n*-C_{25}, and *n*-C_{27} (Kirkels et al., 2013). In particular, a C_{max} of C_{27} has been observed in *Betula* (Schwark et al., 2002; Sachse et al., 2006; Zech et al., 2010; Tarasov et al., 2013; Balascio et al., 2018), *Fagus* (Sachse et al., 2006), and *Quercus* (Kirkels et al., 2013; Lane, 2017) species, all of which were present at PRC during MIS 5d-5a (Minckley et al., 2015). Some *Pinus* species also have a C_{max} of C_{27} (Kirkels et al., 2013 and references therein), and *Pinus* was dominant at PRC during MIS 5d-5a (Minckley et al., 2015). However, *n*-alkane production in *Pinus* species is very low (Diefendorf et al., 2011, 2015; Lane, 2017) and *Pinus* likely did not substantially influence the sedimentary *n*-alkane record despite its potential presence at PRC-South. Further, Freimuth et al. (2019) found that the source of sedimentary *n*-alkanes in a temperate bog was biased towards trees and woody plants, likely due to a combination of intricate mixing processes related to vegetation composition and biomass and wax production. Although we lack an unambiguous record of mid-Holocene vegetation change for PRC, regional pollen records indicate that expansive forests composed primarily of *Pinus* and *Quercus* likely characterized this period (Fletcher et al., 2007). Expansion of these tree species in combination with *Sphagnum* decline at PRC-South and *n*-alkane biases towards trees and other woody plants in bog sediments (Freimuth et al., 2019) could explain irregular molecular distributions and the prominently terrestrial source of C_{23}, C_{25}, and C_{27} *n*-alkanes in Zone 3 that is indicated by higher $\Delta D_{mid\text{-}C29}$ values (Fig. 8).

Terrestrial and *Sphagnum* carbon isotope fractionation differ substantially due to their contrasting physiology, and a largely terrestrial origin of *n*-alkanes in Zone 3 also has significant implications for the interpretation of $\delta^{13}C_{mid}$ values. The fractionation response of non-vascular species, such as *Sphagnum* mosses, to humidity is generally opposite that of vascular plants due to their lack of stomatal conductance. Without guard cells to regulate stomatal aperture, diffusion of gases into the chloroplasts of *Sphagnum* and carbon isotope fractionation are thereby determined by the thickness of a leaf surface water film (Rice, 2000; Loader et al., 2016). A thicker water film resulting from relatively wet conditions inhibits CO_2 diffusion and the preferential utilization of lighter isotopologues is reduced, thus contributing to more positive $\delta^{13}C$ values. Conversely, a thinner water film during dry climatic conditions enhances CO_2 diffusion, which results in more negative $\delta^{13}C$ values (Rice, 2000; Loader et al., 2016). The minimal variations in $\delta^{13}C_{n\text{-alkane}}$ values at PRC-South are likely indicative of changing hydroclimatic conditions rather than relative contributions of C_3 and C_4 vegetation (Taylor et al., 2018), and a largely terrestrial source of mid-chain *n*-alkanes in Zone 3 requires a differential interpretation of $\delta^{13}C_{n\text{-alkane}}$ values from *Sphagnum*-dominated zones.

Although all homologues are primarily terrestrially-derived in Zone 3, trend divergence and small carbon isotopic offsets still exist between middle and long-chain *n*-alkanes at PRC-South. The C_{29} *n*-alkane exhibits a positive $\delta^{13}C$ excursion at 60 cm that is similar, but not as drastic, as that exhibited by $\delta^{13}C_{mid}$ values, while $\delta^{13}C_{n\text{-}C31}$ values remain constant (Fig. 6), likely indicating differences in the terrestrial origin of *n*-alkanes. The $\delta^{13}C_{mid}$ values in Zone 3 are presumably representative of tree species and $\delta^{13}C_{n\text{-}C31}$ values are presumably representative of Ericaceae, which was predominant at the site during MIS 5d-5a (Minckley et al., 2015) and is common in contemporary *Sphagnum* wetlands and in Portugal today (Costa et al., 2000). Ericaceous shrubs, such as *Calluna vulgaris*, often predominantly produce *n*-C_{31} and/or *n*-C_{33} (Ortiz et al., 2011; Kirkels et al., 2013), thus mid-chain and C_{29} *n*-alkanes are likely not primarily derived from Ericaceae. PRC-South $\delta^{13}C_{n\text{-alkane}}$ values vary minimally during the relatively short time period encompassed by the deposit and are overall very similar between middle and long-chain *n*-alkanes (Fig. 6), so climatic interpretations here require little amending. In different *Sphagnum*-inhabited locales, however, inconsistent sources of mid-chain *n*-alkanes combined with the opposing carbon isotope effects of hydrological change in vascular vs. non-vascular species necessitates consideration when interpreting $\delta^{13}C_{mid}$ values.

Overall, $\Delta D_{mid\text{-}C29}$ at PRC-South exemplifies the ambiguity of mid-chain *n*-alkane origin and the uncertainty associated with applications of δD_{mid} and $\delta^{13}C_{mid}$ for paleoclimate reconstructions, regardless of homologue dominance. Qualitative interpretations of δD_{mid} may be dependable, but δD_{mid} values should be carefully assessed prior to quantitative analysis. In the absence of additional, more specific evidence of regional vegetation composition, such as fossil pollen assemblages, $\Delta D_{mid\text{-}C29}$ could be used to improve interpretations of molecular distributions and $\delta^{13}C_{mid}$ values and determine the reliability of δD_{mid} values in *Sphagnum*-dominated paleoenvironments.

5.4. Limitations and future directions

5.4.1. Compound-specific δD variability among terrestrial plant species

Biodiversity is typically low in *Sphagnum* wetlands due to their restrictive sedimentary chemistry (van Breemen, 1995), and isotopic effects of vascular plant variability are likely minimal in such depositional settings (Nichols et al., 2010). Still, there is some potential for terrestrial source variability of long-chain *n*-alkanes that could modify $\delta D_{n\text{-}C29}$ values and reduce the effectiveness of $\Delta D_{mid\text{-}C29}$ for mid-chain *n*-alkane source elucidation. Interspecies $\epsilon_{l/w}$ can differ significantly and is dependent upon a variety of factors including growth form, photosynthetic pathway, plant physiology, microclimate, and biochemistry (Smith and Freeman, 2006; Liu and Yang, 2008; McInerney et al., 2011; Sachse et al., 2012). Within the same catchment area, Hou et al. (2007) reported differences in δD of as much as 70‰ between vegetation types (trees, ferns, grasses, shrubs, etc.), and Balascio et al. (2018) noted similar variability of interspecies isotope fractionation in an ombrotophic bog in northern Norway. At PRC-South, growth form variability could have contributed to some modification of $\delta D_{n\text{-}C29}$ values, particularly as a result of changing *n*-alkane contributions from shrubs and trees. However, the substantial isotopic differences between *Sphagnum* and terrestrial vegetation apparent at PRC-South (as much as 100‰ in Zone 1; Table S1), likely helped to subdue the expression of other growth form isotope effects. Despite its improbable or insignificant influence at PRC-South, terrestrial interspecies δD variability and potential origin ambiguity of long-chain *n*-alkanes (e.g. Rao et al., 2014) should be considered in $\Delta D_{mid\text{-}C29}$ analyses, as it could limit interpretations over certain times scales and at specific sites. Considerable offsets in δD and $\delta^{13}C$ between *n*-alkane chain-lengths from the same species are also common (Balascio et al., 2018; Zhao et al., 2018) and therefore not necessarily indicative of diverse origins. Changes in this isotopic offset over time still have potential value for *n*-alkane source elucidation, but inherent isotopic differences between chain-lengths should additionally be considered.

5.4.2. Hydrogen isotope fractionation and n-alkane production in Sphagnum mosses

Although $\Delta D_{mid\text{-}C29}$ displays a pronounced correspondence to other molecular proxies of vegetation change at PRC-South, our understanding of *Sphagnum* hydrogen isotope fractionation is not yet sufficient for a complete evaluation of the general applicability of $\Delta D_{mid\text{-}C29}$ to *Sphagnum* environments. Few studies have analyzed contemporary *Sphagnum* *n*-alkane δD, and those that have demonstrate sizable measurement differences and variable values between species. Using controlled growth conditions, Nichols et al. (2010) determined that the $\epsilon_{l/w}$ of *n*-C_{23} from *Sphagnum* spp. was approximately −175‰, which is 44‰ lower than the average $\epsilon_{l/w}$ of *Sphagnum* spp. at multiple European sites (Sachse et al., 2006). However, the $\epsilon_{l/w}$ of *Sphagnum* spp. estimated by Sachse et al. (2006) did vary by site, ranging between −140‰ and −120‰. Also using controlled growing conditions, Brader et al. (2010) measured $\delta D_{n\text{-alkane}}$ values of three *Sphagnum* species (*S. fallax*, *S. magellanicum*, and *S. rubellum*) and interspecies δD variability was greater than 30‰. Based on these results, it's likely that *Sphagnum* $\epsilon_{l/w}$ is locale- and species-specific, and $\Delta D_{mid\text{-}C29}$ may not clearly illustrate the changeable origin of mid-chain *n*-alkanes if terrestrial and *Sphagnum* $\epsilon_{l/w}$ are similar, which would depend upon both extant *Sphagnum* species and terrestrial vegetation in a given region. Additionally, given interspecies $\epsilon_{l/w}$ offsets, $\Delta D_{mid\text{-}C29}$ could also reflect changes in *Sphagnum* species composition, but this source variability would likely not correspond to any significant changes in ACL or P_{aq} as *n*-alkane production is relatively similar in most *Sphagnum* mosses, with the exception of species that abundantly produce *n*-C_{31}. Further research into interspecies variability of *Sphagnum* $\delta D_{n\text{-alkane}}$ values would improve not only applications of $\Delta D_{mid\text{-}C29}$, but also paleoclimate interpretations of $\delta D_{n\text{-alkane}}$ values in *Sphagnum* wetlands and peatlands.

Despite the low production of *n*-C_{29} by *Sphagnum* mosses, *n*-C_{29} is still produced to some extent (Bingham et al., 2010) and could alter the interpretation of $\Delta D_{mid\text{-}C29}$. Given a primarily *Sphagnum* origin of *n*-C_{29}, we would not see a considerable isotopic offset between mid-chain homologues and *n*-C_{29} and any visible change in $\Delta D_{mid\text{-}C29}$ related to *Sphagnum* *n*-C_{29} production would likely also have to correspond to significant loss or change in the terrestrial vegetation community. In this case and assuming that the moss still predominantly produced mid-chain homologues, $\Delta D_{mid\text{-}C29}$ values would be close to zero or positive and likely correspond to an increase, rather than a decrease, in P_{aq} or P_{aq27}. While $\Delta D_{mid\text{-}C29}$ values at PRC-South are high at 60 cm, this shift corresponds to a large decrease in P_{aq} to 0.21, and other shifts toward higher values of $\Delta D_{mid\text{-}C29}$ similarly correspond to decreases in mid-chain *n*-alkane relative abundance. A shift in *Sphagnum* moss composition to species with high *n*-C_{29} or *n*-C_{31} production relative to mid-chain *n*-alkanes could produce a similar molecular signal, but this is unlikely given the prevalent production of *n*-C_{29} by terrestrial plant species, which would help to subdue the effects of long-chain production by *Sphagnum*, and the comparably rare production of *n*-C_{29} and *n*-C_{31} by *Sphagnum* mosses. Although uncommon, it is more probable that there are considerable *Sphagnum* contributions to sedimentary *n*-C_{31}, as species such as *S. magellanicum* and *S. capillifolium* predominantly produce this homologue (Nott et al., 2002), but produce *n*-C_{29} to a smaller extent (Bingham et al., 2010 and references therein). As such, $\Delta D_{mid\text{-}C29}$ should vary in response to changes in terrestrial vs. *Sphagnum* moss communities even with some long-chain contributions from *Sphagnum*, although the relationship between $\Delta D_{mid\text{-}C29}$ and molecular proxies would be more difficult to discern.

5.4.3. Microbial n-alkane production

Sedimentary *n*-alkanes are primarily derived from higher plants, but in-situ production of *n*-alkanes by microbes is a necessary consideration in paleoenvironmental applications of leaf wax proxies (Li et al., 2018; Zech et al., 2011). Li et al. (2018) found that microbial *n*-alkane contributions to laboratory incubated peatland soils under aerobic conditions were primarily represented by C_{18}–C_{21} and C_{27}–C_{31} *n*-alkanes with a smaller odd over even predominance than in plants, and only C_{18} and C_{19} *n*-alkanes were produced under anaerobic conditions. In a litterbag experiment, Zech et al. (2011) found microbial production of C_{20}–C_{24} *n*-alkanes in addition to longer chain *n*-alkanes that were also associated with a decline in odd over even predominance. Nonetheless, the findings of Li et al. (2018) indicate that leaf waxes are still viable paleoclimate proxies in anaerobic depositional settings, but more caution should be exercised if sediments are mostly aerobic.

At the PRC-South wetland, anoxic conditions likely limited microbial activity and *n*-alkane production, but following *Sphagnum* decline, the wetland may have experienced some soil aeration. Reduced C/N values coinciding with *Sphagnum* loss in Zone 1 could indicate greater decomposition and microbial activity resulting from the reduction in acidic, waterlogged conditions created in part by *Sphagnum* moss (Taylor et al., 2018). CPI values range from 2.02 to 16.77 at PRC-South, and although variable, ultimately indicate a predominantly higher plant origin of *n*-alkanes with a strong odd over even predominance (Fig. 5). High CPI values do not preclude microbial influence, but it's likely that microbial contributions to sedimentary *n*-alkanes were not extensive enough to significantly alter δD values and negate the use of $\Delta D_{mid\text{-}C29}$. The sampling intervals with lower C/N values (Taylor et al., 2018) that also coincide with large shifts in CPI or relatively low CPI values, such as the transition from Zone 2 to Zone 3, are perhaps more so influenced by microbial activity and degradation (Zech et al., 2013), but these changes in CPI could also be a result of changes in vegetation. In a study of *n*-alkane distributions across various plant groups, Bush and McInerney (2013) documented a wide range of CPI values and suggested that CPI cannot be interpreted solely in terms of *n*-alkane origin or degree of degradation. Further, despite CPI values being variable and low across the transition from Zone 2 to Zone 3, there are no distinct changes in *n*-alkane concentration during the same interval

that might indicate microbial degradation (Zech et al., 2013; Fig. S1). In the upper 40 cm of the deposit there is greater correspondence between CPI values and changes in *n*-alkane concentration (Fig. 5 and Fig. S1), but these larger changes also coincide with relatively large shifts in $ACL_{29\text{-}33}$ (Fig. 5), perhaps indicating an influence of terrestrial vegetation change, degradation, or a combination of the two. Given that CPI values at PRC-South overall follow trends in molecular proxies of vegetation composition more closely (Fig. 5), we interpret changes in terrestrial plant *n*-alkane origin to be the primary factor driving changes in CPI, with degradation and microbial contributions as additional modifying factors.

If microbial activity was a significant source of sedimentary *n*-alkanes, it is still unclear what effect it would have on $\Delta D_{mid\text{-}C29}$. Fractionation factors for microbes have not been established, and *n*-alkane degradation by microbes vs. *n*-alkane production by microbes have opposing influences on sedimentary compound-specific δD values. Biodegradation results in an apparent D-enrichment of *n*-alkanes, which primarily affects short-chain ($< C_{19}$) waxes (Pond et al., 2002), and microbial *n*-alkane contributions are relatively D-depleted likely because soil rather than leaf water is used for biosynthesis (Zech et al., 2011). Additionally, with some microbial communities only producing short- and long-chain *n*-alkanes (Li et al., 2018) and others producing both mid- and long-chain *n*-alkanes (Zech et al., 2011), the importance of microbial contributions for $\Delta D_{mid\text{-}C29}$ applications varies with microbial community and is difficult to assess. Microorganism *n*-alkane production and alteration of sedimentary δD values is understandably an essential consideration, but if it does not appear to impede upon paleoclimate applications of long-chain δD values, the use of $\Delta D_{mid\text{-}C29}$ is likely justifiable.

6. Conclusion

Interspecies variability of hydrogen isotope fractionation in plants is a considerable source of uncertainty in paleoenvironmental reconstructions that utilize the $\delta D_{n\text{-alkane}}$ proxy, as compositional modification of sedimentary $\delta D_{n\text{-alkane}}$ values may be interpreted as hydrological change. Source variability of a particular *n*-alkane is typically inferred from fossil pollen analyses in order to determine or correct for species-specific isotope fractionation (e.g. Feakins, 2013; Lane et al., 2018) but in the absence of pollen data, other methods of *n*-alkane source elucidation should be explored. At PRC-South, we employed the difference in δD between mid-chain and C_{29} *n*-alkanes ($\Delta D_{mid\text{-}C29}$) in attempt to disentangle mid-chain and C_{27} *n*-alkane origin in an initially *Sphagnum*-dominated wetland. Strong correspondence between each $\Delta D_{mid\text{-}C29}$ series and molecular *n*-alkane proxies (P_{aq}, P_{aq27}) illustrate the significant influence of vegetation change on δD_{mid} values. Although the effects of vegetation variability on δD_{mid} values are likely magnified at PRC-South due to both rapid, substantial change and large isotopic offsets between regional *Sphagnum* and terrestrial plant species, $\Delta D_{mid\text{-}C29}$ exemplifies the importance of accounting for the effects of vegetation composition on $\delta D_{n\text{-alkane}}$ values. Fractionation processes that alter the hydrogen isotope composition of *Sphagnum*-derived *n*-alkanes are difficult to infer given the current literature, and additional investigations into interspecies *Sphagnum* $\epsilon_{l/w}$ are needed to accurately interpret *Sphagnum* $\delta D_{n\text{-alkane}}$ values and thoroughly evaluate the general paleoenvironmental utility of $\Delta D_{mid\text{-}C29}$ in *Sphagnum* wetlands.

Declarations of interest

None.

Acknowledgements

The US National Science Foundation provided funding for fieldwork in Portugal (BCS-1118183 and BCS-1420453) and compound-specific isotope analyses (EAR-1427494). The UNCW Center for Marine Science and the UNCW Center for the Support of Undergraduate Research and Fellowships provided additional funding for instrument analyses. We appreciate the student crew that assisted with sampling of the wetland deposit in 2013 and Kimberley Rosov for analytical assistance.

Appendix A. Supplementary data

Supplementary data to this article can be found online at https://doi.org/10.1016/j.quaint.2019.09.009.

References

Aichner, B., Herzschuh, U., Wilkes, H., 2010a. Influence of aquatic macrophytes on the stable carbon isotopic signatures of sedimentary organic matter in lakes on the Tibetan Plateau. Org. Geochem. 41 (7), 706–718. https://doi.org/10.1016/j.orggeochem.2010.02.002.

Aichner, B., Herzschuh, U., Wilkes, H., Vieth, A., Böhner, J., 2010b. δD values of *n*-alkanes in Tibetan lake sediments and aquatic macrophytes – a surface sediment study and application to a 16ka record from Lake Koucha. Org. Geochem. 41 (8), 779–790. https://doi.org/10.1016/j.orggeochem.2010.05.010.

Baas, M., Pancost, R., van Geel, B., Sinninghe Damsté, J.S., 2000. A comparative study of lipids in *Sphagnum* species. Org. Geochem. 31 (6), 535–541. https://doi.org/10.1016/S0146-6380(00)00037-1.

Balascio, N.L., D'Andrea, W.J., Anderson, R.S., Wickler, S., 2018. Influence of vegetation type on *n*-alkane composition and hydrogen isotope values from a high latitude ombrotrophic bog. Org. Geochem. 121, 48–57. https://doi.org/10.1016/j.orggeochem.2018.03.008.

Benedetti, M.M., Haws, J.A., Funk, C.L., Daniels, J.M., Hesp, P.A., Bicho, N.F., et al., 2009. Late Pleistocene raised beaches of coastal Estremadura, central Portugal. Quat. Sci. Rev. 28 (27), 3428–3447. https://doi.org/10.1016/j.quascirev.2009.09.029.

Bingham, E.M., McClymont, E.L., Väliranta, M., Mauquoy, D., Roberts, Z., Chambers, F.M., et al., 2010. Conservative composition of *n*-alkane biomarkers in *Sphagnum* species: implications for palaeoclimate reconstruction in ombrotrophic peat bogs. Org. Geochem. 41 (2), 214–220. https://doi.org/10.1016/j.orggeochem.2009.06.010.

Brader, A.V., van Winden, J.F., Bohncke, S.J.P., Beets, C.J., Reichart, G.-J., de Leeuw, J.W., 2010. Fractionation of hydrogen, oxygen and carbon isotopes in *n*-alkanes and cellulose of three *Sphagnum* species. Org. Geochem. 41 (12), 1277–1284. https://doi.org/10.1016/j.orggeochem.2010.09.006.

Bush, R.T., McInerney, F.A., 2013. Leaf wax *n*-alkane distributions in and across modern plants: Implications for paleoecology and chemotaxonomy. Geochimica et Cosmochimica Acta 117, 161–179. https://doi.org/10.1016/j.gca.2013.04.016.

Chikaraishi, Y., Naraoka, H., 2003. Compound-specific δD–$\delta^{13}C$ analyses of *n*-alkanes extracted from terrestrial and aquatic plants. Phytochemistry 63 (3), 361–371. https://doi.org/10.1016/S0031-9422(02)00749-5.

Diefendorf, A.F., Freeman, K.H., Wing, S.L., Graham, H.V., 2011. Production of *n*-alkyl lipids in living plants and implications for the geologic past. Geochem. Cosmochim. Acta 75 (23), 7472–7485. https://doi.org/10.1016/j.gca.2011.09.028.

Diefendorf, A.F., Leslie, A.B., Wing, S.L., 2015. Leaf wax composition and carbon isotopes vary among major conifer groups. Geochem. Cosmochim. Acta 170, 145–156. https://doi.org/10.1016/j.gca.2015.08.018.

Diefendorf, A.F., Freimuth, E.J., 2017. Extracting the most from terrestrial plant-derived *n*-alkyl lipids and their carbon isotopes from the sedimentary record: a review. Org. Geochem. 103, 1–21. https://doi.org/10.1016/j.orggeochem.2016.10.016.

Eglinton, G., Hamilton, R.J., 1967. Leaf epicuticular waxes. Science 156 (3780), 1322–1335. https://doi.org/10.1126/science.156.3780.1322.

Feakins, S.J., 2013. Pollen-corrected leaf wax D/H reconstructions of northeast African hydrological changes during the late Miocene. Palaeogeogr. Palaeoclimatol. Palaeoecol. 374, 62–71. https://doi.org/10.1016/j.palaeo.2013.01.004.

Ficken, K., Li, B., Swain, D., Eglinton, G., 2000. An *n*-alkane proxy for the sedimentary input of submerged/floating freshwater aquatic macrophytes. Org. Geochem. 31 (7), 745–749. https://doi.org/10.1016/S0146-6380(00)00081-4.

Fletcher, W.J., Boski, T., Moura, D., 2007. Palynological evidence for environmental and climatic change in the lower Guadiana valley, Portugal, during the last 13 000 years. Holocene 17 (4), 481–494. https://doi.org/10.1177/0959683607077027.

Freimuth, E.J., Diefendorf, A.F., Lowell, T.V., Wiles, G.C., 2019. Sedimentary *n*-alkanes and *n*-alkanoic acids in a temperate bog are biased toward woody plants. Org. Geochem. 128, 94–107. https://doi.org/10.1016/j.orggeochem.2019.01.006.

Haws, J.A., Benedetti, M.M., Funk, C.L., Bicho, N.F., Daniels, J.M., Hesp, P.A., et al., 2010. Coastal wetlands and the Neanderthal settlement of Portuguese Estremadura. Geoarchaeology 25 (6), 709–744. https://doi.org/10.1002/gea.20330.

Hepp, J., Wüthrich, L., Bromm, T., Bliedtner, M., Schäfer, I.K., Glaser, B., et al., 2019. How dry was the younger dryas? Evidence from a coupled δ2H–δ18O biomarker paleohygrometer applied to the Gemündener maar sediments, western Eifel, Germany. Clim. Past 15 (2), 713–733. https://doi.org/10.5194/cp-15-713-2019.

Hou, J., D'Andrea, W.J., MacDonald, D., Huang, Y., 2007. Hydrogen isotopic variability in leaf waxes among terrestrial and aquatic plants around Blood Pond, Massachusetts (USA). Org. Geochem. 38 (6), 977–984. https://doi.org/10.1016/j.orggeochem.2006.12.009.

Kahmen, A., Hoffmann, B., Schefuß, E., Arndt, S.K., Cernusak, L.A., West, J.B., Sachse, D., 2013a. Leaf water deuterium enrichment shapes leaf wax *n*-alkane δD values of angiosperm plants II: observational evidence and global implications. Hydrogen

Isotopes 111, 50–63. https://doi.org/10.1016/j.gca.2012.09.004.
Kahmen, A., Schefuß, E., Sachse, D., 2013b. Leaf water deuterium enrichment shapes leaf wax *n*-alkane δD values of angiosperm plants I: experimental evidence and mechanistic insights. Hydrogen Isotopes 111, 39–49. https://doi.org/10.1016/j.gca.2012.09.003.
Kirkels, F.M., Jansen, B., Kalbitz, K., 2013. Consistency of plant-specific *n*-alkane patterns in plaggen ecosystems: a review. Holocene 23 (9), 1355–1368. https://doi.org/10.1177/0959683613486943.
Lane, C.S., 2017. Modern *n*-alkane abundances and isotopic composition of vegetation in a gymnosperm-dominated ecosystem of the southeastern U.S. coastal plain. Org. Geochem. 105, 33–36. https://doi.org/10.1016/j.orggeochem.2016.12.003.
Lane, C.S., Taylor, A.K., Spencer, J., Jones, K.B., 2018. Compound-specific isotope records of late-quaternary environmental change in southeastern North Carolina. Quat. Sci. Rev. 182, 48–64. https://doi.org/10.1016/j.quascirev.2017.12.022.
Li, G., Li, L., Tarozo, R., Longo, W.M., Wang, K.J., Dong, H., Huang, Y., 2018. Microbial production of long-chain *n*-alkanes: implication for interpreting sedimentary leaf wax signals. Org. Geochem. 115, 24–31. https://doi.org/10.1016/j.orggeochem.2017.10.005.
Liu, W., Yang, H., Wang, H., An, Z., Wang, Z., Leng, Q., 2015. Carbon isotope composition of long chain leaf wax *n*-alkanes in lake sediments: a dual indicator of paleoenvironment in the Qinghai-Tibet Plateau. Org. Geochem. 83 (84), 190–201. https://doi.org/10.1016/j.orggeochem.2015.03.017.
Liu, J., An, Z., 2019. Variations in hydrogen isotopic fractionation in higher plants and sediments across different latitudes: implications for paleohydrological reconstruction. Sci. Total Environ. 650, 470–478. https://doi.org/10.1016/j.scitotenv.2018.09.047.
Loader, N.J., Street-Perrott, F.A., Mauquoy, D., Roland, T.P., van Bellen, S., Daley, T.J., et al., 2016. Measurements of hydrogen, oxygen and carbon isotope variability in *Sphagnum* moss along a micro-topographical gradient in a southern Patagonian peatland. J. Quat. Sci. 31 (4), 426–435. https://doi.org/10.1002/jqs.2871.
Marzi, R., Torkelson, B.E., Olson, R.K., 1993. A revised carbon preference index. Org. Geochem. 20 (8), 1303–1306. https://doi.org/10.1016/0146-6380(93)90016-5.
McInerney, F.A., Helliker, B.R., Freeman, K.H., 2011. Hydrogen isotope ratios of leaf wax *n*-alkanes in grasses are insensitive to transpiration. Geochem. Cosmochim. Acta 75 (2), 541–554. https://doi.org/10.1016/j.gca.2010.10.022.
Minckley, T.A., Haws, J.A., Benedetti, M.M., Brewer, S.C., Forman, S.L., 2015. Last interglacial vegetation and climate history from the Portuguese coast. J. Quat. Sci. 30 (1), 59–69. https://doi.org/10.1002/jqs.2758.
Mügler, I., Sachse, D., Werner, M., Xu, B., Wu, G., Yao, T., Gleixner, G., 2008. Effect of lake evaporation on δD values of lacustrine *n*-alkanes: a comparison of Nam Co (Tibetan Plateau) and Holzmaar (Germany. Org. Geochem. 39 (6), 711–729. https://doi.org/10.1016/j.orggeochem.2008.02.008.
Nichols, J.E., Booth, R.K., Jackson, S.T., Pendall, E.G., Huang, Y., 2006. Paleohydrologic reconstruction based on *n*-alkane distributions in ombrotrophic peat. Org. Geochem. 37 (11), 1505–1513. https://doi.org/10.1016/j.orggeochem.2006.06.020.
Nichols, J., Booth, R.K., Jackson, S.T., Pendall, E.G., Huang, Y., 2010. Differential hydrogen isotopic ratios of *Sphagnum* and vascular plant biomarkers in ombrotrophic peatlands as a quantitative proxy for precipitation—evaporation balance. Geochem. Cosmochim. Acta 74 (4), 1407–1416. https://doi.org/10.1016/j.gca.2009.11.012.
Nott, C.J., Xie, S., Avsejs, L.A., Maddy, D., Chambers, F.M., Evershed, R.P., 2000. *n*-Alkane distributions in ombrotrophic mires as indicators of vegetation change related to climatic variation. Org. Geochem. 31 (2), 231–235. https://doi.org/10.1016/S0146-6380(99)00153-9.
Ortiz, J.E., Díaz-Bautista, A., Aldasoro, J.J., Torres, T., Gallego, J.L.R., Moreno, L., Estébanez, B., 2011. *n*-Alkan-2-ones in peat-forming plants from the Roñanzas ombrotrophic bog (Asturias, northern Spain). Org. Geochem. 42 (6), 586–592. https://doi.org/10.1016/j.orggeochem.2011.04.009.
Polissar, P., J.D'Andrea, W., 2014. Uncertainty in paleohydrologic reconstructions from molecular δD values. Geochem. Cosmochim. Acta 129 (15), 145–156. https://doi.org/10.1016/j.gca.2013.12.021.
Pond, K.L., Huang, Y., Wang, Y., Kulpa, C.F., 2002. Hydrogen isotopic composition of individual *n*-alkanes as an intrinsic tracer for bioremediation and source identification of petroleum contamination. Environ. Sci. Technol. 36 (4), 724–728. https://doi.org/10.1021/es011140r.
Rach, O., Brauer, A., Wilkes, H., Sachse, D., 2014. Delayed hydrological response to Greenland cooling at the onset of the Younger Dryas in western Europe. Nat. Geosci. 7, 109.
Rach, O., Kahmen, A., Brauer, A., Sachse, D., 2017. A dual-biomarker approach for quantification of changes in relative humidity from sedimentary lipid D/H ratios. Clim. Past 13 (7), 741–757. https://doi.org/10.5194/cp-13-741-2017.
Rao, Z., Jia, G., Qiang, M., Zhao, Y., 2014. Assessment of the difference between mid- and long chain compound specific δD *n*-alkanes values in lacustrine sediments as a paleoclimatic indicator. Org. Geochem. 76, 104–117. https://doi.org/10.1016/j.orggeochem.2014.07.015.
Rice, S.K., 2000. Variation in carbon isotope discrimination within and among *Sphagnum* species in a temperate wetland. Oecologia 123 (1), 1–8.
Sachse, D., Radke, J., Gleixner, G., 2004. Hydrogen isotope ratios of recent lacustrine sedimentary *n*-alkanes record modern climate variability. Geochem. Cosmochim. Acta 68 (23), 4877–4889. https://doi.org/10.1016/j.gca.2004.06.004.
Sachse, D., Radke, J., Gleixner, G., 2006. δD values of individual *n*-alkanes from terrestrial plants along a climatic gradient – implications for the sedimentary biomarker record. Org. Geochem. 37 (4), 469–483. https://doi.org/10.1016/j.orggeochem.2005.12.003.
Sachse, D., Billault, I., Bowen, G.J., Chikaraishi, Y., Dawson, T.E., Feakins, S.J., et al., 2012. Molecular paleohydrology: interpreting the hydrogen-isotopic composition of lipid biomarkers from photosynthesizing organisms. Annu. Rev. Earth Planet Sci. 40 (1), 221–249. https://doi.org/10.1146/annurev-earth-042711-105535.
Schwark, L., Zink, K., Lechterbeck, J., 2002. Reconstruction of postglacial to early Holocene vegetation history in terrestrial Central Europe via cuticular lipid biomarkers and pollen records from lake sediments. Geology 30 (5), 463–466. https://doi.org/10.1130/0091-7613(2002)030<0463:ROPTEH>2.0.CO;2.
Seki, O., Meyers, P.A., Kawamura, K., Zheng, Y., Zhou, W., 2009. Hydrogen isotopic ratios of plant wax *n*-alkanes in a peat bog deposited in northeast China during the last 16kyr. Org. Geochem. 40 (6), 671–677. https://doi.org/10.1016/j.orggeochem.2009.03.007.
Séneca, A., 2003. The genus *Sphagnum* L. in Portugal. Cryptogam. Bryol. 24 (2), 103–126.
Sousa, A., Morales, J., García-Barrón, L., García-Murillo, P., 2012. Changes in the Erica ciliaris Loefl. ex L. peat bogs of southwestern Europe from the 17th to the 20th centuries ad. Holocene 23 (2), 255–269. https://doi.org/10.1177/0959683612455545.
Tarasov, P.E., Müller, S., Zech, M., Andreeva, D., Diekmann, B., Leipe, C., 2013. Last glacial vegetation reconstructions in the extreme-continental eastern Asia: potentials of pollen and *n*-alkane biomarker analyses. Quat. Int. 290–291, 253–263. https://doi.org/10.1016/j.quaint.2012.04.007.
Taylor, A.K., Benedetti, M.M., Haws, J.A., Lane, C.S., 2018. Mid-Holocene Iberian hydroclimate variability and paleoenvironmental change: molecular and isotopic insights from Praia Rei Cortiço, Portugal. J. Quat. Sci. 33 (1), 79–92. https://doi.org/10.1002/jqs.3000.
van Breemen, N., 1995. How *Sphagnum* bogs down other plants. Trends Ecol. Evol. 10 (7), 270–275. https://doi.org/10.1016/0169-5347(95)90007-1.
Zech, M., Andreev, A., Zech, R., Müller, S., Hambach, U., Frechen, M., Zech, W., 2010. Quaternary vegetation changes derived from a loess-like permafrost palaeosol sequence in northeast Siberia using alkane biomarker and pollen analyses. Boreas 39 (3), 540–550. https://doi.org/10.1111/j.1502-3885.2009.00132.x.
Zech, M., Pedentchouk, N., Buggle, B., Leiber, K., Kalbitz, K., Marković, S.B., Glaser, B., 2011. Effect of leaf litter degradation and seasonality on D/H isotope ratios of *n*-alkane biomarkers. Geochem. Cosmochim. Acta 75 (17), 4917–4928. https://doi.org/10.1016/j.gca.2011.06.006.
Zech, M., Krause, T., Meszner, S., Faust, D., 2013. Incorrect when uncorrected: reconstructing vegetation history using n-alkane biomarkers in loess-paleosol sequences – a case study from the Saxonian loess region, Germany. Quat. Int. 296, 108–116. https://doi.org/10.1016/j.quaint.2012.01.023.
Zhao, B., Zhang, Y., Huang, X., Qiu, R., Zhang, Z., Meyers, P.A., 2018. Comparison of *n*-alkane molecular, carbon and hydrogen isotope compositions of different types of plants in the Dajiuhu peatland, central China. Org. Geochem. 124, 1–11. https://doi.org/10.1016/j.orggeochem.2018.07.008.